Journal of Hydrology 615 (2022) 128610

Contents lists available at ScienceDirect

Journal of Hydrology

journal homepage: www.elsevier.com/locate/jhydrol

Research papers

The impacts of near-bed flow characteristics on river bed sediment transport under ice-covered conditions in 2016–2021

Eliisa Lotsari [a,b,*], Karoliina Lintunen [c], Elina Kasvi [c], Petteri Alho [c,d], Linnea Blåfield [c]

[a] Water and Environmental Engineering, Department of Built Environment, Aalto University, P.O. Box 15200, Tietotie 1E, 00076 Aalto, Finland
[b] Department of Geographical and Historical Studies, University of Eastern Finland, Yliopistokatu 2, P.O. Box 111, FI-80101 Joensuu, Finland
[c] Department of Geography and Geology, University of Turku, FI-20014 Turun yliopisto, Turku, Finland
[d] Finnish Geospatial Research Institute FGI, National Land Survey of Finland, Vuorimiehentie 5, FI-02150 Espoo, Finland

ARTICLE INFO

This manuscript was handled by Marco Borga, Editor-in-Chief, with the assistance of Luca Mao, Associate Editor

Keywords:
Ice-covered flow
Near-bed velocity
Sediment transport
Time series analysis
Subarctic
Finland

ABSTRACT

Global climate change has been projected to affect hydrology, the ice-covered flow period and river morphology (including changed sediment transport conditions) in northern high-latitude regions. To understand the impact of the expected shortening of the ice-covered period on bedload transport, one needs to understand the present sediment transport in these high-latitude rivers with annually occurring ice cover. Thus, the aims are (1) to define the impacts of ice cover on near-bed flow characteristics during hydrologically varying years, and (2) to analyse the impacts of these mid-winter flow characteristics on the bed sediment transport potential. The analyses are based on Acoustic Doppler Current Profiler (ADCP: 2016–21) and Acoustic Doppler Velocimeter (ADV: 2020–21) measurements performed in mid-winter ice-covered conditions of the sandy and small (circa 20 m wide) Pulmanki River in northern Finnish Lapland.

Despite the ice-covered river conditions in winter, sediment transport occurs even during these harshest mid-winter conditions. The critical velocities and shear velocities of mid-winter conditions were exceeded in winters 2016–2021, and bedload transport occurred according to bedload measurements. Three different situations occurred regarding the bed sediment transport and near-bed velocity conditions: (1) high measured mid-winter discharges indicate high velocities throughout the meander bend; (2) low measured mid-winter discharges cause low near-bed velocities throughout the meander bend; (3) winters having intermediate discharges indicate near-bed velocities and sediment transport potential being higher at the upstream inlet and apex sections of the meander bend but clearly lower downstream of the apex. The confinement by the river ice cover, i.e. bottom-fast ice, explains the velocity variation. The near-bed velocities were the highest at the upstream inlet section of a symmetrical meander bend, where the measurement cross-sections were narrower and shallower. The velocities were the lowest downstream of the apex, where the channel changed from relatively narrow to wider and deeper.

1. Introduction

Due to global climate change, rapid changes are occurring especially in northern high-latitude regions (IPCC, 2021). The warming has been projected to affect hydrology, the ice-covered flow period and river morphology, including changed sediment transport conditions (Syvitski, 2002; Kämäri et al., 2015, 2018; Song et al., 2019; IPCC, 2021). The duration of the frozen (and unfrozen) periods, including river-ice cover and its properties, may affect the sediment transport characteristics. However, according to Lotsari et al. (2015a) in their review of reach-scale river simulation approaches to future in-channel changes, overall there had been very few modelling approaches, and none of the reviewed papers had included river ice cover (cf. Table 1 of Lotsari et al., 2015a). The enormous and risky work required for measuring the flow and sediment transport potential in ice-covered conditions has been one of the factors influencing the availability of data for calibrating models for present and future simulations. Thus, to understand the impacts of the expected future shortening of the frozen period (Prowse et al., 2011; Turcotte et al., 2011; Lind et al., 2016) on sediment transport (including bedload) and before being able to perform reliable future modelling, an

* Corresponding author at: Water and Environmental Engineering, Department of Built Environment, Aalto University, P.O. Box 15200, Tietotie 1E, 00076 Aalto, Finland.
E-mail addresses: eliisa.s.lotsari@aalto.fi (E. Lotsari), emklin@utu.fi (K. Lintunen), elina.kasvi@utu.fi (E. Kasvi), mipeal@utu.fi (P. Alho), linnea.m.blafield@utu.fi (L. Blåfield).

https://doi.org/10.1016/j.jhydrol.2022.128610
Received 28 January 2022; Received in revised form 15 August 2022; Accepted 23 September 2022
Available online 30 October 2022
0022-1694/© 2022 The Authors. Published by Elsevier B.V. This is an open access article under the CC BY license (http://creativecommons.org/licenses/by/4.0/).

understanding is needed of the present sediment transport conditions in different high-latitude northern rivers with annually occurring ice cover. Long-term data series would enable these analyses.

At the watershed scale, studies of the northern rivers and their sediment transport have mainly concentrated on large Arctic rivers (e.g. Lena, Mackenzie, Ob, Yenisey). The smaller watersheds have received less focus (Lewis and Lamoureux, 2010) even though they cover the majority of the land area north of 60° latitude. These smaller watersheds respond to fast hydrological changes as the small lake percentage and connectivity of the river network usually enable a relatively quick flow through the system (Veijalainen et al., 2010; Kämäri et al., 2015). This makes them ideal for measuring the annual variability in the river ice cover and magnitude of the related sediment transport process, especially within this northern zone of the most rapid climate change (Syvitski, 2002; IPCC, 2021). In high-latitude, low-turbidity rivers, bedload can be a major transport process, especially during the low flow periods of the ice-covered season. As many watershed-scale sediment load analyses have mainly focused on the suspended load instead of including bedload, new insights into reach-scale sediment transport are needed before analysing at the watershed scale or projecting into the future (Ladegaard-Pedersen et al., 2017).

Recent studies have shown that the ice-covered flow season can have a significant impact on river bed sediment transport (Tremblay et al., 2014; Lotsari et al., 2015b; Polvi et al, 2020). Studies on suspended sediment transport in ice-covered conditions also exist from previous (Prowse 1993; Ettema and Daly, 2004) and recent decades, and analytical methods based on acoustic signals have recently appeared (Moore et al., 2013; Weiss et al., 2015). However, more studies on reach-scale ice-covered bed sediment transport processes are especially still needed from a variety of river ice conditions before being able to fully understand the complex flow, ice and sediment transport interactions in different river systems.

The measurements under ice cover are possible via drillholes (Lotsari et al., 2017) for analysing simultaneous flow velocities and bedload transport conditions. These ice-covered flow and bedload transport conditions can be detected by applying standard equipment such as Acoustic Doppler Current Profilers (ADCP) and mechanical Helley-Smith bedload samplers (Helley and Smith, 1971; Lotsari et al., 2017, 2019a). The Helley-Smith sampler and ADCP continuous moving boat measurement (with bottom track) have been simultaneously used for measuring bedload conditions in an open channel flow (Rennie et al., 2002; Gaeuman and Jacobson, 2006; Rennie et al., 2017). Relationships between bedload and bed velocity (i.e. sediment movement) parameters could also be made in ice-free seasons (Gaeuman and Jacobson, 2006). The presence of ice cover makes transport processes more complicated than in open-channel conditions because the roughness of the ice cover has an impact on the flow area and velocities. Recent research on the ice-covered flow of natural rivers (i.e. not laboratory environments) has shown that the high-velocity cores are closer to the river bed under the ice cover than in open-channel conditions (e.g. Demers et al., 2011; Lotsari et al., 2017). In a laboratory study by Wang et al. (2008), the location of the maximum velocity has been shown to move to the bed. This is consistent with the studies done in natural rivers by Demers et al. (2011) and Lotsari et al. (2017) regarding high-velocity core locations. Wang et al. (2008) had also shown in the laboratory that for the same flow depth, the near-bed velocity under the ice cover is clearly higher than that in the open channel flow. Further, in natural rivers, the river ice (especially during severe winters and under low-flow conditions) can cause the flow to concentrate only within the deepest and highest velocity portion of the channel (Prowse, 1996).

This may impact the sediment transport (including the bedload) despite the overall low flow conditions during the ice-covered season when compared to other seasons (Lotsari et al., 2019b). However, the ice cover has been shown to reduce the sediment transport through decreasing velocity, bed shear stress and diffusivity (Prowse, 1996). According to Beltaos and Burrell (2016), the ice cover changes the flow velocity and shear stress, but it also affects changes in vertical diffusivity and longitudinal dispersion, further affecting the spread of suspended substances. Studies on the impacts of the ice cover on sediment transport are rarer in natural rivers than in laboratory experiments. However, a few studies do exist. For example, the shear forces exerted on the river bed have been shown to increase when the ice thickness and especially its roughness increase (Kämäri et al., 2015). Based on the study of Kämäri et al. (2015) done with a one-dimensional hydraulic model (HEC-RAS), a smooth, thermally formed 5–40 cm thick ice cover overall decreased the average shear stress compared to an open water situation. Also, changes in boundary shear stress and flow resistance have been analysed based on the ice cover (Zare et al., 2016a, b; Biron et al., 2019). Zare et al. (2016a) showed that ice deposition and erosion can occur during the stable ice cover period as a result of flow variations induced by hydropeaking. They also showed that commonly employed assumptions about ice and bed zone velocity values, hydraulic radii and energy grade line slopes are inaccurate in these cases. Further, Zare et al. (2016b) studied the shear stress imposed on the boundaries of a natural ice-covered river, especially during different ice stages, and demonstrated that the bed shear stress during the ice cover period is less than during the open water condition, which proves that the upper boundary layer (i.e. the ice cover) presence has a diminishing effect on bed shear stress. However, recent publications using acoustic analyses and dealing with river bed resistance in ice-covered conditions, such as Zare et al. (2016a), have often been done only from one spatial location of the river channel, and cross-sectional or spatially varying data and analyses between years have not been detected.

In laboratory conditions, Namaee and Sui (2019) studied the role of critical dimensionless shear stress, grain size and roughness of ice cover on the incipient motion of bed material around bridge piers. They found that the ice cover can cause a deeper maximum scour depth than in open-channel flow conditions, and also the required flow velocity for the incipient motion of sediment particles under the ice cover decreases with an increase in the relative roughness coefficient of the ice cover (Namaee and Sui, 2019). Also, Wang et al. (2008) concluded based on their laboratory study that if the ratio between the ice cover resistance coefficient to the resistance coefficient of channel bed increases, then the location of the maximum velocity moves to the bed. Due to the complex observed impacts of the ice cover on sediment transport processes in both natural and laboratory river experiments—and the lack of studies concentrating especially on bedload transport in natural (i.e. non-laboratory) rivers—the impact of hydrologically different winters and their varying ice-cover conditions on near-bed velocities and the expected bedload transport requires further attention.

The long time series of ice-covered flow and bedload sediment transport conditions are rare in northern high-latitude rivers. One of them is the Pulmanki River in northern Finnish Lapland, where ice-covered mid-winter conditions have been measured systematically for several years. The subarctic study region is within the area of the fastest projected future climatic change and is central for analysing the following impacts of hydrological variability and changes. Thus, this unique data series from the years 2016–2021 makes the Pulmanki River an ideal location for analysing the varying mid-winter conditions on the near-bed flow characteristics and their potential for the sediment transport in the ice-covered season. The aims of this paper are (1) to define the impacts of ice cover on near-bed flow characteristics during hydrologically varying years and (2) to analyse the impacts of these mid-winter flow characteristics on the bed sediment transport potential. Near-bed velocity means the velocity measured closest to the river bed (within the limits of the equipment). The analyses are based on ADCP (2016–21) and Acoustic Doppler Velocimeter (ADV: 2020–21) measurements performed in mid-winter ice-covered conditions at the Pulmanki River in northern Finnish Lapland.

2. Study site

The study site is located at the meandering Pulmanki River, which is a tributary of the Tana River (Fig. 1). The Pulmanki River is divided into two parts by Lake Pulmanki. The watershed area of the upper Pulmanki River is 484 km^2. This study concentrates on one simple symmetric meander bend of the upper Pulmanki River. Its radius of curvature and width of the curvature at the apex are 110 m and 19 m, respectively (Lotsari et al., 2014).

The climate of northern Finnish Lapland is influenced both by the Atlantic Ocean, heated by the Gulf Stream, and the great Asian continent in the east (Autio and Heikkinen, 2002). Therefore, this area belongs to the Köppen climate class: 'Cold, without dry season, but with cold summer'. The Pulmanki River typically freezes in October when the temperature drops below 0 °C (Peel et al., 2007; Lotsari et al., 2019b). Temperatures start to rise above 0 °C again in early April, and the freezing period can last approximately-seven months (Lotsari et al., 2019b). The temperatures usually reach −30 to −40 °C sometime during the period of December–February (Figs. 2 and 3 in Lotsari et al., 2019b). The Pulmanki River had a smooth-rough ice cover during the analysed years when defined visually from photos and ice blocks lifted onto the ice surface, following Demers et al. (2013), Lotsari et al. (2017), and Kämäri et al. (2017). This was similar to mid-winters in 2014 and 2015 analysed by Kämäri et al. (2017) and Lotsari et al. (2017, 2019a, 2019b). Annual maximum discharges occur during spring snowmelt events when discharges typically rise to 50 m^3/s (Kasvi et al., 2013). This typically occurs between mid-May and early June. During summer, discharges are around 4 m^3/s, and less than 2 m^3/s discharges have been measured during autumn and winter (Lotsari et al., 2019a).

The river runs through glaciolacustrine and glacio-fluvial sediments, which had been deposited after the ice-dammed lake had drained during the final wasting of the Fennoscandian ice sheet (Hirvas et al., 1988; Johansson, 1995, 2007; Lotsari et al., 2020a). The D_{50} values of the river bank material have been measured to range from approximately 0.004 mm to 0.529 mm and the friction angle of the material to be 35–36.5° (cf. for a detailed description of the banks' sediment and figures of ice-free conditions from Lotsari et al., 2020a), making the sediment highly mobile. Consolidated sediment does not appear in the area where there is active river activity. There, the material is loose sand and gravel. For example, a high bank studied by Lotsari et al. (2020a) includes 1.5–16 m of loose, very well-sorted fluvial sand with weak soil development in the upper 0.3 m. In addition, roots are only causing cohesion at the top of the bank within 0.5 m depth. The bulk density of channel bank sediment is 1.73 g/cm^3. The bed load is the main mode of transport, as the suspended sediment amount is small, even during the spring snow-melt discharge periods (cf. Lotsari et al., 2020b).

3. Methods

3.1. Near-bed velocity measurements

The flow velocity was measured in 2016–2021 cross-sectionally with an Acoustic Doppler Current Profiler (ADCP, M9 sensor, Sontek) (Table 1). The M9 sensor has both four 3.0 MHz beams and four 1.5 MHz beams. The sensor is accurate up to +/−0.25 % of the measured velocity (+/−0.2 cm/s) (Sontek, 2015). Within the cross-sections, each measurement hole was drilled about 1 m apart from each other. The measurements always began from the left bank and moved towards the right bank. The ice depths were measured before the sensor was placed through the holes of the ice cover. There were some measurement verticals where the water depth was too shallow for measurements, and therefore only the ice thickness was measured from those locations. The stationary mode of the M9 sensor was applied, i.e. it produces the time-averaged value of each measured parameter at each measurement drillhole location. The mid-section method was selected for discharge measurements, and the averaging time was set to 60 s at each drill hole. We selected this time-averaged method each year to avoid the macro-turbulent impact of the river flow (Lotsari et al., 2020b), i.e. for gaining the time-averaged flow parameters directly from the sensor and also for comparing the data between years. The sensor, which had been

Table 1
The measurement times and used equipment. The ADCP measurements were all done in stationary mode, and the averaging time in the mid-section method was 60 s each time. The FlowTracker was used where the water depth was too shallow for the ADCP.

Measurement dates	ADCP M9: cs1–4 and csA–C	FlowTracker: cs1–4	Discharge (m^3/s)
16.02.2016	x		1.38
16.02.2017	x		1.32
09.02.2018	x		0.18
07.02.2019	x		0.61
05.02.2020	x	x	0.79
15.02.2021	x	x	0.496

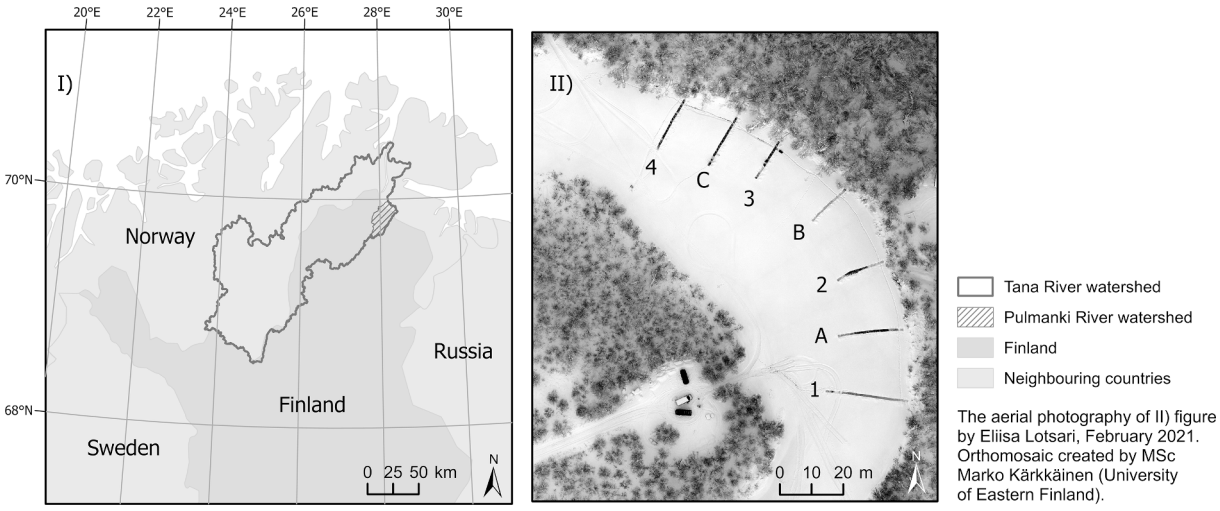

Fig. 1. The study site of the Pulmanki River. (I) The Pulmanki River watershed within its larger geographical content. (II) Close view of the studied meander bend of the upper Pulmanki River. The orthomosaic (aerial photos by Eliisa Lotsari; orthomosaic processing by Marko Kärkkäinen, University of Eastern Finland) is from 15 Feb 2021, with measurement cross-sections visible. Holes for measurements were drilled in each cross-section about 1 m apart, starting from the left bank to the right bank. The river runs northward, and the cross-section (cs) 1 is the most upstream measurement location.

mounted on a metal rod, was lowered at the level of ice cover water interface before initiating the measurements at each drillhole. The tagline azimuth was defined before the ADCP measurement at the first drillhole of each cross-section. A vertical beam was used as the depth reference. The transducer depth of the sensor was set as 0 m to maximise the flow measurement area in the vertical direction in this shallow water environment and to include all possible effects of the ice cover and river bed. As a result of these ADCP measurements, the spatial and vertical variations in flow velocity and flow depth were gained from each of the drilled holes within the measurement cross-sections. The ADCP calculates the total velocity of each cell based on the following equation:

$$\sqrt{x^2 + y^2 + z^2} \quad (1)$$

where x, y and z represent the velocities in the three different directions.

The near-bed velocities, i.e. the measured total velocity of the cells closest to the river bed, were extracted from the data sets. The height of the measured cells from the river bed was also derived based on the depth of the cell and the total measured depth of each measurement vertical.

In some of the measurement points, the water depth was too shallow for the ADCP, as it requires around 25 cm of water. Thus, from these measurement verticals, Sontek's FlowTracker (a side-looking ADV, Acoustic Doppler Velocimeter) was instead applied to measure the velocity close to the river bed. The FlowTracker makes a point measurement, whereas ADCP velocities are obtained over the spatial domain of the acoustic beams. The FlowTracker was placed as close to the river bed as possible, i.e. the sensor's lower edge was ~3 cm above the river bed each time. The sensor has ~5 cm vertical height, and the upper limit of the measurements was each time around 8 cm up from the river bed. The measurement height from the river bed coincided with most of the near-bed velocity cell heights measured with the ADCP (cf. Results section). The FlowTracker measurements were done in the same cross-sections as the ADCP measurements (Table 1). Note that the mid-section discharge measurement mode was not used in the case of the FlowTracker. Instead, each point measurement was a separate 50-second long measurement. For making the data set comparable with the ADCP data (as the FlowTracker gives the results in x, y and z directions), the total velocities of each FlowTracker measurement were calculated using Eq. (1). The near-bed velocities measured with the ADCP and FlowTracker were then compared from year to year at each cross-section.

3.2. The analyses of the sediment transport and related near-bed flow characteristics

The near-bed flow velocities of each winter were also compared against the critical fluvial forces capable of initiating the bedload movement. This also required analyses of the grain sizes of the transported bedload material, which were measured in the winters of 2020 and 2021. The Helley-Smith sampler (Helley and Smith, 1971) was applied for mechanically measuring the bedload transport on 6 February 2020 and 18 February 2021 (Table 2). The measurements were aimed to take each time from the high flow location of that cross-section (i.e. in the middle or at the left bank side of cs1) and at the outer bank side of the other cross-sections cs2, cs3 and cs4. Note that no measurements were taken from csA, csB or csC. The intake opening of the sampler was 77 mm. Each sample was taken for 6 min each time. Each sample was dried in the oven (105 °C) and weighted. The bedload was calculated with Eq. (2) (cf. Morales et al., 2019), where G is the dry weight (kg), b is the intake opening (m) and T is the measurement time (min).

$$G/(b^*T) \quad (2)$$

The grain size distribution of each sample was analysed via dry-sieving and by using sieves having half-phi interval mesh sizes. The D_{10}, D_{50} and D_{90} values were calculated in addition to defining the textural group. In the winter of 2020, two samples were large enough for dry-sieving. In the winter of 2021, six samples were large enough for dry sieving (Table 2). We did not include the unsieved samples in this study. The average D_{50} value of all sieved samples was calculated, as these are the basis for the bedload movement analyses. The average D_{50} grain size of all bedload samples was 0.5383 mm in the winter of 2021 and 0.6076 mm in the winter of 2020. Overall, the average D_{50} grain size of all samples in 2020 and 2021 had been 0.5557 mm. The average D_{90} value was 1.1341 mm. This average D_{50} value of 0.5557 mm was used in the equations for analysing whether the mid-winter near-bed velocities were capable of exceeding the critical forces needed to move these sized particles from all analysed years.

In addition, for gaining the spatial distribution of the grain sizes of the river bed, the Van Veen bulk bed sediment sampler was applied to get a more detailed distribution of the river bed material. The samples were taken from the right, middle and left bank locations at each cross-section in 2020 October. These were thus measured between the mid-winter 2020 and mid-winter 2021 measurement times, and these river bed material conditions can be expected to best represent the distribution of the 2020 and 2021 mid-winter bed material. The average D_{50} and D_{90} sediment grain size values were calculated for each cross-section. The D_{50} values were then used for analysing whether the mid-winter 2020 and 2021 velocities exceeded the critical thresholds for moving the sediment. These data were not applied in the analyses of previous years to avoid uncertainties, as the bed material might have been different in 2016–2019. Thus, the average D_{50} value of 0.5557 mm (based on Helley-Smith samples) was used for all years.

The traditional Hjulström (1935) critical velocity for transport (lower line) would have been 0.035 m/s for 0.5557-mm sized particles, i.e. for the average D_{50} value of Helley-Smith bedload samples. The comparative critical velocity for erosion (Hjulström, 1935) would have been 0.275 m/s. In addition to comparing the exceeding of these thresholds for motion, other methods were also applied. For selecting the methods for analysing flow characteristics and their impact on bed sediment transport, various previous publications of open-channel and under-ice particle motion studies were checked, especially the ones done in ice-covered laboratory experiments and which have not yet been tested widely in real river environments. These included publications related to the densimetric Froude number for incipient motion of sediment (Wang et al. 2008 [eqs. (4) and (5)]; Hirshfield and Sui, 2011). However, for being able to define the sediment particle motion as much as possible based on the measured data sets, the Wang et al. (2008) method was discarded as the parameters such as the roughness

Table 2
The grain sizes analysed based on the 2020 and 2021 winter bedload (Helley-Smith) samples. cs = cross-section. Measurement time of each sample was 6 min.

Date	cs, sample no.	D_{10} (mm)	D_{50} (mm)	D_{90} (mm)	Textural group	Bedload (mg/(m*s))	Total sample dry weight (g)
18.2.2021	cs1, 1	0.3169	0.5081	0.9894	Slightly Gravelly Sand; 99.4 % sand	4801.587	133.1
18.2.2021	cs1, 2	0.3602	0.5854	1.1543	Slightly Gravelly Sand; 99.3 % sand	6713.564	186.1
18.2.2021	cs1, 3	0.3384	0.5575	1.2189	Slightly Gravelly Sand; 97 % sand	721.501	20.0
18.2.2021	cs2, 1	0.2909	0.4927	1.0568	Slightly Gravelly Sand; 99.5 % sand	1356.421	18.8
18.2.2021	cs2, 2	0.2838	0.5055	1.2711	Slightly Gravelly Sand; 96.2 % sand	1035.354	28.7
18.2.2021	cs4, 1	0.3649	0.5811	1.0342	Sand; 100 % sand	137.085	3.8
6.2.2020	cs1, 1	0.2703	0.4274	0.9267	Slightly Gravelly Sand; 99.5 % sand	772.006	21.4
6.2.2020	cs4, 1	0.4388	0.7877	1.4212	Slightly Gravelly Sand; 98.3 % sand	5324.675	147.6

coefficient of ice cover (n_i) and the roughness coefficient (Manning's n; n_b) of the channel bed would have been needed to be estimated, which would have caused more uncertainties to the analyses. Also, we did not apply the direct moving bed analysis method based on the ADCP's bottom track, such as by Rennie et al. (2002), as our data had the output only in time-averaged format (single value from each drillhole) due to the stationary discharge measurement mode, which had also been selected for minimizing the possible effect of macro-turbulence (Lotsari et al., 2020). We also discarded the methods that would have included parameters that we would not have data for a detailed definition and which would have caused further uncertainties. Under the ice cover, for example, the definition of the local slope is uncertain. This cross-sectional gradient definition for streamwise velocity would have affected the results (Zare et al., 2016b). Zare et al. (2016) also presented different ways to calculate boundary shear stress, one of them including a method without the slope effect (based on maximum and average velocities and the von Karman constant: Eq. (7) of theirs). However, we did not select this method for our use as it had been originally defined based on a bottom-mounted ADCP for gaining the local boundary shear stress on both upper (ice-water interface) and lower (river bed) boundaries and not for detecting the motion of particles similar in size to the Pulmanki River material. In addition the "bed shear velocity related to grains" approach of Van Rijn (1984) was discarded, as it would have made the results cross-sectionally averaged due to the applied mean velocity. That approach would have also required calculation of Chezy equation with hydraulic radius parameter, which would have been an approximation, and would have caused further uncertainties.

Namaee and Sui (2019) had used in their ice-covered laboratory experiments logarithmic equation for defining the shear forces (their Eq. (9)). This equation has been previously been applied for defining the shear velocity from direct flow measurements (Wilcock, 1996; Sime et al., 2007). According to Wilcock (1996), using a single near-bed velocity observations in the equation are less precise than if depth-averaged velocity in the vertically averaged logarithmic velocity profile is applied instead. However, Wilcock (1996) states that this method requires appropriate flow conditions only near the bed, so it may be applied in a wider range of flow conditions, including spatially variable flow. Also, according to Rhoads (2020), this law of the wall in question can be applied for local shear analyses at channel boundary. Sime et al. (2007) applied the same equation, and state that Wilcock (1996) results were for time-averaged velocities at a particular set of measurement heights at a single site, and not instantaneous ADCP measurements. As our data is time-averaged and from various spatial locations, the Wilcock (1996) approach, where the single velocity measurements had been applied for shear velocity (u_*) calculation was selected. Thus, we selected the approach which allowed the calculation of shear velocity exactly for the measured velocity value closest to the river bed.

For calculating critical shear velocity, we selected to use a parameterization of the Shield's (Shields, 1936) curve, more precisely decided to follow the Van Rijn (1984) approach where non-dimensional grain size D_* is applied. After defining both the observed shear velocity (u_*) and the critical shear velocity (u_{*c}), the transport stage parameter (Van Rijn, 1984) was defined by comparing the resulting shear velocity and critical shear velocities. Also Namaee and Sui (2019) had applied this transport stage parameter in their under ice laboratory experiments.

Thus, first the particle parameter (D_*) was calculated with Eq. (3) (Van Rijn, 1984: their Eq. (1)):

$$D_* = D_{50}\left[\frac{(S-1)g}{\nu^2}\right]^{\frac{1}{3}} \tag{3}$$

where s is specific density and calculated as ρ_s/ρ. ρ is the mass density of water (0.99987 g/cm^3 or 999870 g/m^3 in zero Celsius degree water temperature). As we had no other mineralogical knowledge of the sediment, ρ_s was defined as a quartz density of 2.65 g/cm^3, common for sand sizes in the majority of natural streams. g is the gravitational acceleration, which is 9.826 m/s^2 in the study area of Northern Finland (Poutanen et al. 2017). v is the kinematic viscosity coefficient defined as (μ/ρ), i.e. based on dynamic viscosity coefficient (μ). However, as for 0°temperature water, the kinematic viscosity coefficient is known to be 1.7930 mm^2/s (Kestin et al., 1978), we applied this value directly. D_{50} value of the sediment particle was 0.5557 mm, as it is the average value for the transported bedload based on Helley-Smith measurements. In addition, the D_* was also calculated based on the average D_{50} value of each cross-section's bed sediment, which had been sampled in October 2020 (Table 3).

Then the critical mobility parameter (θ_{cr}) was defined based on the equation defined at Fig. 1 of Van Rijn (1984). The equation was selected based on the D_* values defined for applied grain sizes. For the 0.5557 mm particles (average of Helley-Smith bedload samples), the D_* was 9.530 and the following equation was selected for θ_{cr}:

$$\theta_{cr} = 0.14(D_*)^{-0.64} \tag{4}$$

The resulting critical mobility parameter value was 0.033. This is used for calculating the critical shear velocity, and further transport stage parameter for all cross-sections of each studied year.

When calculating the critical mobility parameter based on the autumn 2020 bulk bed sediment samples of each cross-section, the same equation (Eq. (4)) was applicable for cs1, cs3 and cs4, but for the cross-sections csA, cs2, csB and csC the equation for D_* values between 10 and 20 was applicable (cf. D_* values Table 3):

$$\theta_{cr} = 0.04(D_*)^{-0.10} \tag{5}$$

The resulting critical mobility parameter values are presented in Table 3. These are applied for calculating the critical shear velocities, and further transport stage parameter for winters 2020 and 2021.

Next the critical shear velocity u_{*c} was solved from the equation Eq. (6) and (7) (Van Rijn, 1984):

$$\theta_{cr} = \frac{{u_{*c}}^2}{(s-1)gD_{50}} \tag{6}$$

which can be written in the form:

$$u_{*c} = \sqrt{\theta_{cr}((s-1)gD_{50})} \tag{7}$$

The resulted critical shear velocities (m/s) were 0.017, based on the average grain sizes of Helley-Smith samples. The critical shear velocities based on the autumn 2020 cross-sectional sediment data are presented in Table 3.

According to Wilcock (1996) the logarithmic relation between the shear velocity u_* and the variation of velocity u with height z above bed is as follows (Eq. (8)).

$$\frac{u}{u_*} = \frac{1}{\kappa} ln\left(\frac{z}{z_0}\right) \tag{8}$$

From this equation the shear velocity can be resolved, when writing the equation in the following form:

$$u_* = \frac{u\kappa}{ln\left(\frac{z}{z_0}\right)} \tag{9}$$

u is the variation of velocity with height z above the bed (Wilcock, 1996). According to Wilcock (1996) single observation of u can be used to estimate u_*, which we also here now-on name as u_{*z}. In our study, as mentioned above, the u is the time-averaged near-bed velocity, i.e. measured within 50–60 s with ADCP or ADV. Despite being single observation, it represents velocity variation within 50–60 s. The measurements of ours were mostly within the lowest 20 % of the water column, thus making the application of this equation as valid (cf. Wilcock, 1996). Only at the following locations the measurement had been slightly more than 20 % of the full depth from the river bed: in 2016 one location at csA; in 2018 two locations at cs1, 6 locations at cs2 and 10

Table 3
The D_{50} and D_{90} values defined from the Van Veen (VV) bulk bed sediment samples measured in autumn 2020 from the study area. cs = cross-section.

	D_{50} values (mm)				Van Rijn (1984)			
	Right bank	Middle	Left bank	Average	non-dimensional grain-size (D_*) of average D_{50}	Critical mobility parameter (θ_{cr}, Eq. (4))	Critical mobility parameter (θ_{cr}, Eq. (5))	Critical shear velocity (u_{*c}, m/s, Eq. (7))
cs1	0.216	0.605	0.544	0.455	7.803	0.038		0.018
csA	0.390	0.426	1.285	0.700	12.005		0.031	0.017
cs2	0.495	0.644	1.302	0.813	13.943		0.031	0.017
csB	0.545	0.637	0.595	0.592	10.153		0.032	0.017
cs3	0.482	0.487	0.187	0.385	6.603	0.042		0.019
csC	0.934	0.487	0.559	0.660	11.319		0.031	0.017
cs4	0.379	0.382	0.366	0.376	6.448	0.043		0.020

	D90 values (mm)			
	Right bank	Middle	Left bank	Average
cs1	0.415	2.050	1.255	1.240
csA	2.028	0.741	5.431	2.733
cs2	1.006	1.702	4.420	2.376
csB	1.144	1.663	2.426	1.744
cs3	0.941	1.003	0.299	0.748
csC	1.985	1.106	3.245	2.112
cs4	0.926	0.911	0.724	0.854

locations at csB; in 2019 one location at csA and one at cs4; in 2020 two locations at csA; and in 2021 one location at cs1. However, for the unity of the results, we calculated the values also for these locations based on the same equation. κ is the von Karman's constant defined 0.4, similarly to Namaee and Sui (2019) and Wilcock (1996).

The z_0 is the bed roughness length, corresponding to u = 0. Wilcock (1996) had calculated it for gravel particles with equation $aD_{84}/30$, where a = 3. Also Sime et al. (2007) had followed Wilcock (1996), and stated that $z_0 = 0.1D_{84}$. However, Sime et al. (2007) also state that for well-sorted uniformly packed sediment $z_0 = D_{50}/30$. Note that their study was based on moving boat ADCP measurements, not time-averaged stationary measurements, as ours are. According to Rhoads (2020) the law of the wall in question can be applied for local shear analyses at channel boundary. They state that in these cases the common method, for defining whether or not at least some portion of the lower part of the turbulent boundary layer exhibits a logarithmic profile, and for solving the shear velocity and also the bed roughness length (z_0), has been to measure mean velocities at several different heights above the bed over the lowest 15–20 % of the flow depth and using the resulting data to fit in linear regression analyses. However, our data does not have several measurements within this 15–20 % layer, and our shear velocity analyses are therefore based on one measured velocity of the cell closest to the river bed. This scarcity of data from bottom layer, as ADCP inherently leaves cells partially or fully touching the river bed unmeasured (as in our data set) due to potential data contamination or potential side-lobe interference, was the reason why Gaeuman and Jacobson (2004) state that accurate estimates of the height of zero-velocity (z_0) flow cannot be obtained from ADCP data. Rhoads (2020) states also that an alternate approach for eliminating the need for this linear regression analysis is to define a relation between z_0 and particle size, such as for example Wilcock (1996) and Sime et al. (2007) had done. The D_{84} sediment sizes mentioned in Sime et al. (2007) are from 17 mm to 82 mm, thus making the sediment much larger than in our study site (cf. the D90 values from Table 3). Our sediment sizes are well sorted sand or gravelly sand, i.e. smaller than gravel or pebbles (Table 2). Due to these reasons, we decided to follow the approach of Namaee and Sui (2019), whose study had been done in ice-covered laboratory conditions, and had applied particles from 0.47, 0.5 and 0.58 mm in their experiments. Our D_{50} value of Helley-Smith samples fell within this range. Also they had depth of flow as 1.3 m, which is close to the maximum measured water depths of Pulmanki river in winters (c.f. Supplementary material). Namaee and Sui (2019) stated that z_0 can be represented as roughness height, which is the D_{50} value of the sediment particle. Thus, due to the similarities to the experimental study conditions of Namaee and Sui (2019), we applied 0.5557 mm as z_0, as it is the average value for the transported bedload based on Helley-Smith measurements. This was used for calculating data sets from all years. In addition, the shear velocity for the years 2020 and 2021 was calculated as a test based on the average D_{50} value of each cross-section's bed sediment, which had been sampled in October 2020 (Table 3).

Finally, the transport stage parameter was calculated based on Eq. (10) (Van Rijn, 1984: their equation (2)).

$$T = \frac{{u_{*z}}^2 - {u_{*c}}^2}{{u_{*c}}^2} \quad (10)$$

This shows the transport capacity based on how much there is excess shear velocity, greater than the critical shear velocity. If the value is negative, there is no excess shear velocity to enable transport.

The calculations were done for each measurement location at each cross-section of each mid-winter situation in 2016–2021. The calculated shear velocity (derived based on the above equations from original ADCP and FlowTracker data) of each measurement location was compared to the critical shear velocity (cf. the full results are presented in Supplementary material, Excel format). The spatial particle transport potential of each winter was analysed from these data sets. In comparison to shear velocity analyses, the near-bed velocities were analysed against the critical velocity threshold of Hjulström (1935), i.e. whether or not the near-bed velocity was greater than the defined threshold.

In addition, the explanatory factors of water depth (full depth below ice) and ice cover thickness were used against near-bed velocities, shear velocities and transport stage parameters in Pearson's correlation analysis to estimate the linear relationship between the normally distributed variables. Based on the assumptions of Pearson's correlation, the method was suitable for the analyses of our data. The results of the Pearson's correlation analysis can vary between −1 and 1, either indicating a negative or positive linear relationship between variables. Values close to zero indicate a low correlation between variables.

4. Results

4.1. The near-bed flow characteristics of 2016–2021 mid-winter conditions

Overall, the near-bed velocities were slow in different winter conditions in 2016–2021 (Fig. 2). The years 2021, 2020 and 2019 had mostly higher velocities at the upstream cross-sections cs1–csB, such as

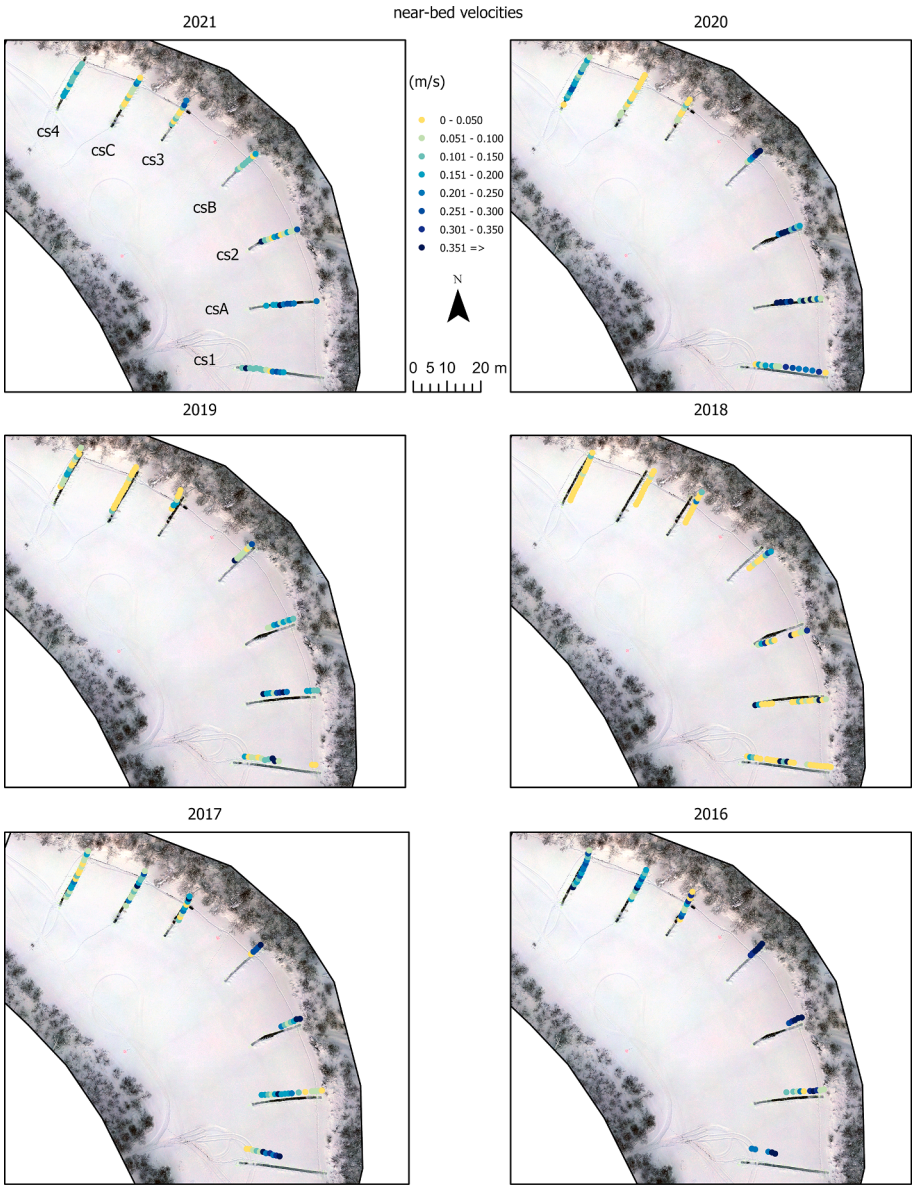

Fig. 2. The near-bed velocities of each year. The aerial photograph is from winter 2021 (by Eliisa Lotsari).

over 0.2–0.3 m/s. Lower velocities, i.e. less than 0.15 m/s, occurred more often at cs3–cs4. In 2018, the near-bed velocities of each cross-section were less than 0.1 m/s in most of the measurement verticals. The overall lowest discharge of the studied years, 0.18 m^3/s (Table 1), explains this difference. The first two winters, 2016 and 2017, had discharges of 1.38 and 1.32 m^3/s, respectively, and thus were very much comparable to each other. The near-bed velocities were also most consistently the highest in those years, i.e. over 0.2 m/s velocities occurred in the three most downstream-located cross-sections. However, cs1 (inlet), cs2 and csB (apex) had the highest near-bed velocities, being over 0.25 m/s and, in many verticals, over 0.3 m/s. The near-bed velocities were the highest at the left bank side at cs1 of the inlet area and close to the outer bank side at cs2 and csB. Thus, three different mid-winter conditions were observed (Table 1, Fig. 2): (1) very low discharge and near-bed velocities occurred in 2018, when the near-bed velocities were low throughout the meander bend; (2) two higher mid-winter discharge conditions were present in 2016 and 2017, and velocities were higher throughout the meander bend; (3) the three last years (2019–2021) had intermediate discharges of 0.5–0.79 m^3/s, and velocities had been clearly divided between 'higher velocities' at the upstream inlet and the apex sections and 'lower velocities' at the downstream outlet section.

When comparing different years, the lowest near-bed velocities occurred most frequently within the cross sections 3 and C. These cross-sections locate where the cross-sectional width, area and flow depth increase after a narrower and shallower reach (Table 4, cf. depths from Supplementary material). The river channel had been confined by the river ice in a way that in the upstream part of the meander bend (approximately at cs1–cs2), the channel had been narrower due to mid-channel bars and bottom-fast ice during many winters (i.e. not possible to measure with the ADCP and thus no location measured, cf. Fig. 2). Also, the flow had been diverted next to the outer bank in narrow cross-sections of the apex area, which also caused higher velocities in several years. The width and area of the measurement cross-sections can be seen in Fig. 2 and Table 4. Thus, after flowing from the narrow csB towards the more downstream cross-sections, the river widened and deepened, and slower near-bed velocities occurred. Unfortunately, we do not have data from the actual pressure conditions from each winter, i.e. whether or not the flow was pressurised. When drilling the ice cover, there was no artesian well style surge of water on top of the ice in any of the cross-

Table 4
The average, maximum and minimum distances from the river bed of near-bed velocities and the magnitudes of flow. Bolded numbers are the cross-section widths that had been the narrowest in each year. The cross-section area means the area of freely flowing water under ice. In case there had been a middle bar within the cross-section, the area from both the left and right bank sides of the middle bar is presented if both sides of the bar were possible to measure with the ADCP/ADV. Note that the cross-section width represents the whole cross-section, including the middle bar where ice was attached to the river bed.

	Year	Cross-section width (m)	Cross-section area (m^2: if middle bar, left + right bank side)	Maximum distance from river bed (m)	Minimum distance from river bed (m)	Average distance from river bed (m)	Percentage of distance from river bed under 0.05 *m*	Maximum near-bed velocity (m/s)	Minimum near-bed velocity (m/s)	Average near-bed velocity (m/s)
cs1	2016	22	2.67 (2.59 + 0.08)	0.08	0.03	0.05	80.0	0.60	0.20	0.34
	2017	22	5.68 (5.48 + 0.2)	0.05	0.01	0.03	100.0	0.62	0.04	0.22
	2018	22	7.1	0.19	0.01	0.09	22.7	0.54	0.00	0.08
	2019	24	4.94 (4.3 + 0.64)	0.08	0.00	0.03	92.9	0.56	0.00	0.13
	2020	24	5.25	0.04	0.01	0.02	100.0	0.33	0.03	0.18
	2021	12	3.55	0.14	0.01	0.05	69.2	0.37	0.04	0.16
csA	2016	18	4.03	0.19	0.01	0.05	70.0	0.38	0.04	0.18
	2017	21	6.49	0.08	0.01	0.04	68.8	0.39	0.03	0.14
	2018	16	4.37	0.30	0.02	0.13	29.4	0.51	0.00	0.10
	2019	17	4.38 (2.33 + 2.05)	0.19	0.03	0.08	41.7	1.16	0.10	0.28
	2020	18	4.66	0.15	0.01	0.06	66.7	1.75	0.07	0.58
	2021	19	4.75	0.24	0.02	0.09	33.3	0.70	0.17	0.27
cs2	2016	**6**	2.37	0.11	0.03	0.07	40.0	0.54	0.25	0.40
	2017	9	4.54	0.14	0.02	0.06	42.9	0.36	0.08	0.20
	2018	11	3.83	0.45	0.07	0.17	0.0	0.69	0.00	0.17
	2019	10	4.67	0.15	0.01	0.05	77.8	0.21	0.05	0.14
	2020	10	3.65	0.16	0.02	0.09	25.0	2.53	0.10	0.59
	2021	12	4.37	0.16	0.01	0.05	75.0	0.75	0.03	0.17
csB	2016	8	3.39	0.12	0.02	0.06	50.0	0.57	0.30	0.42
	2017	**7**	4.82	0.30	0.01	0.10	40.0	0.36	0.01	0.24
	2018	**8**	3.52	0.26	0.15	0.18	0.0	0.26	0.01	0.08
	2019	8	5.39	0.11	0.04	0.07	37.5	1.56	0.02	0.29
	2020	**9**	3.83	0.14	0.02	0.08	33.3	0.55	0.06	0.28
	2021	**10**	3.86	0.08	0.01	0.03	87.5	0.18	0.03	0.11
cs3	2016	10	5.32	0.14	0.01	0.05	80.0	0.34	0.02	0.16
	2017	9	6.13	0.22	0.02	0.08	44.4	0.39	0.01	0.16
	2018	10	6.45	0.22	0.03	0.10	18.2	0.23	0.00	0.05
	2019	**6**	7.51	0.19	0.01	0.13	14.3	0.20	0.01	0.07
	2020	**9**	4.82	0.11	0.01	0.05	62.5	0.12	0.00	0.05
	2021	**10**	6.9	0.19	0.01	0.06	66.7	0.26	0.02	0.10
csC	2016	12	6.45	0.19	0.06	0.10	0.0	0.60	0.07	0.20
	2017	13	6.52	0.13	0.01	0.05	75.0	1.25	0.05	0.22
	2018	12	6.06	0.11	0.03	0.06	50.0	0.05	0.00	0.02
	2019	16	7.46	0.09	0.01	0.05	62.5	0.13	0.00	0.03
	2020	16	5.71	0.07	0.01	0.03	92.9	0.12	0.00	0.04
	2021	12	6.92	0.14	0.01	0.04	72.7	0.21	0.01	0.09
cs4	2016	14	5.4	0.15	0.01	0.05	61.5	0.36	0.09	0.21
	2017	19	7.29	0.18	0.01	0.04	81.3	0.23	0.02	0.10
	2018	16	5.56	0.08	0.01	0.03	88.2	0.11	0.00	0.02
	2019	13	6.06	0.26	0.03	0.10	35.7	0.19	0.01	0.08
	2020	16	5.35	0.10	0.02	0.06	43.8	0.28	0.00	0.15
	2021	12	4.62	0.05	0.02	0.03	100.0	0.20	0.06	0.14

sections during the measurement years, thus more likely indicating non-pressurised conditions.

The differences and similarities between the locations of maximum near-bed velocities were possible to detect during years 2016–2021 (Fig. 3). The maximum velocities were especially clustered at the left bank side at cs1 and the outer bank at csB and cs3. The most variation between years had been at csA and csC over the years (Fig. 3). The mid-channel bar at cs1 existed only in 2020, 2017 and 2016. However, in 2018, the mid-channel bar had influenced the division of flow at cs1, csA and cs2, and the location of maximum velocity varied that year the most from the other years between these cross-sections. In 2020, the mid-channel bar had located at cs1 and csA. On the contrary, the flow had been possible to measure in mid-winter 2021 throughout all cross-sections. Thus, the mid-channel bars had not influenced the division of the flow around the bar at that time.

The variations in near-bed velocity (Fig. 2), shear velocity (cf. Supplementary material) and transport stage parameter (Fig. 4) were analysed against explaining factors of depth (full water depth below the ice) and ice cover thickness (Tables 5 and 6). When the annual connections were analysed (Table 5), all Pearson correlation values show very little correlation between any parameters. The highest positive correlations occurred in 2016 (0.41) and 2021 (0.39) between depth and ice thickness, and only twice was there a negative correlation greater than −0.30, which occurred in 2020 between ice thickness and near-bed velocity (-0.32) and ice thickness and shear velocity (-0.34). All other parameters and years correlated closer to zero. Thus, basically no

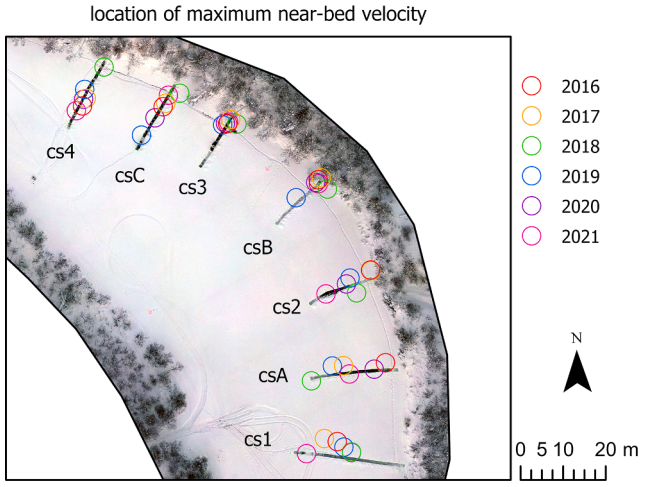

Fig. 3. The locations of maximum near-bed velocities of all measurement time steps.

correlation occurred when depth was compared to shear velocity or transport stage parameter. Similarly correlation values were mostly very low when ice thickness was compared to shear velocity or transport stage parameter. The application of different D_{50} values as the basis of the calculations had no clear effect on the results (Table 5). Despite being generally low correlation coefficients, in 2016, all correlations were positive. In 2017, there was negative correlation when ice thickness was applied in analyses against near-bed velocity, shear velocity and transport stage parameter, but positive correlation when depth was applied in the analyses. Only in 2018 the correlation between depth and ice thickness was negative (i.e. the greater the depth, the thinner the ice thickness), in other years the value was positive. The correlation coefficient between depth and shear velocity or transport stage parameter, and ice-thickness and shear velocity or transport stage parameter, were mostly negative, i.e. the greater the depth or ice thickness, the smaller the shear velocity and transport stage parameter.

Table 6 explains this situation of very low annual correlation values, as it shows the correlation between the parameters separately within each cross-section. There is great variation in the direction of correlation between different cross-sections during certain mid-winter measurement times, but differences also occurred between years for certain

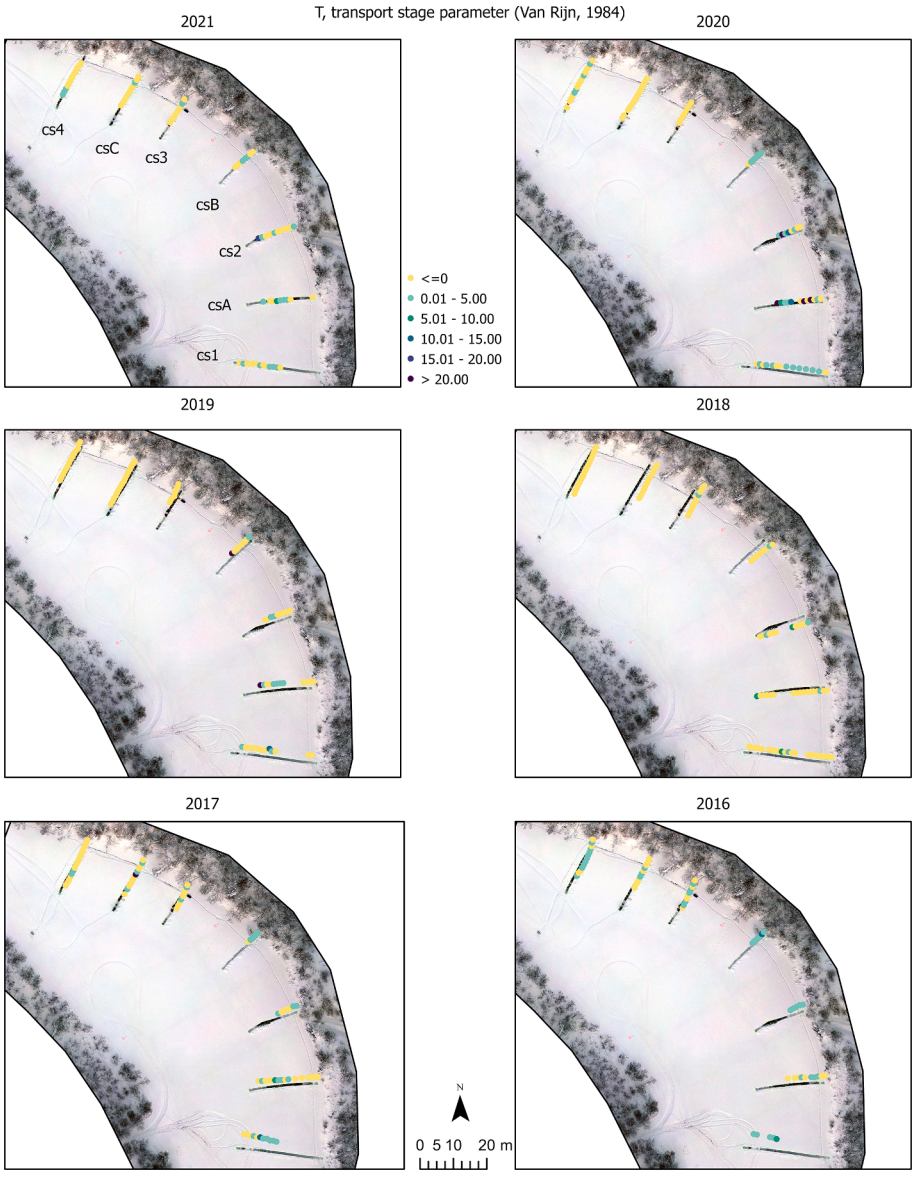

Fig. 4. Transport stage parameter of each measurement time. The aerial photograph is from winter 2021 (Eliisa Lotsari).

Table 5
The Pearson correlation coefficients between different parameters during each mid-winter measurement time. The depth in the calculations is the full water depth (below ice) of the measurement vertical.

Year	Depth vs ice thickness	Depth vs near bed velocity	Depth vs shear velocity	Depth vs transport stage parameter	Ice thickness vs near-bed velocity	Ice thickness vs shear velocity	Ice thickness vs transport stage parameter
Average D_{50} of bedload samples used							
2016	0.41	0.24	0.14	0.17	0.11	0.16	0.12
2017	0.08	0.20	0.09	0.06	−0.22	−0.24	−0.10
2018	−0.27	0.00	−0.03	−0.05	−0.27	−0.28	−0.18
2019	0.07	−0.16	−0.18	−0.15	0.05	0.06	0.04
2020	0.04	−0.22	−0.28	−0.20	−0.32	−0.34	−0.25
2021	0.39	−0.13	−0.18	−0.13	−0.13	−0.09	−0.05
Cross-sectional D_{50} used							
2020			−0.27	−0.19		−0.34	−0.25
2021			−0.17	−0.12		−0.06	−0.03

cross-sections. CsB, which locates at the apex and which has been the narrowest cross-section in four out of six mid-winter measurement times (Table 4), has high correlation in most of the years when depth is used in the correlation analyses. Only in 2021, the correlation between depth and near-bed velocity, shear velocity or transport stage parameter had been very low. When ice thickness was applied in the analyses, high correlation occurred with ice-thickness in years 2016–2018 and 2020 at csB. The years 2021 and 2019, which had lower correlations, belong to the 'intermediate discharge magnitude' mid-winter conditions, when there had been clearly higher velocities at the upstream and apex sections and lower near-bed velocities at the downstream measurement locations. When ice thickness was analysed against shear velocity or transport stage parameter at csB, only in 2018 and 2020 the correlations were clearly high and negative (-0.72 or more at each case), meaning that the greater the ice thickness had been, the smaller the shear velocity or transport stage parameter had been. At csB, the correlation between depth and the near-bed velocity is mainly positive, i.e. the greater the depth, the greater the near-bed velocities. On the other hand, the correlation between the ice thickness and the near-bed velocities is negative in each year. Also, the ice thickness and depth have a negative correlation at csB in most of the years. Thus, the greater the ice thickness, the smaller the depth and near-bed velocities.

In addition to high correlation values occurring at csB, the greatest correlation values at cs1 and cs2 (Table 6) occurred most often between different parameters in 2016, which was considered to have 'high discharge' conditions. During the year 2017, which also had relatively high mid-winter discharges, there had been high correlation values at cs2 between most of the compared parameter pairs. Only when ice thickness had been compared against shear velocity or transport stage parameter, the correlation had been lower, i.e. around −0.31– −0.32 at cs2. There is a clear change when detecting the three downstream-most cross-sections at the outlet area. The most often high correlations occurred between parameters in the 2019 and 2021 'intermediate discharge' years at cs3. Also at csC, the highest correlation values of most parameter pairs occurred in 2021. At cs4, it is noteworthy that this is the only cross-section where the 'low discharge' mid-winter year in 2018 most often had a high correlation between parameter pairs. The applied grain size had no or very little (i.e. around 0.01) impact on the correlation values (Table 6), except in 2021 at cs3 the correlation values had been 0.03–0.05 greater when cross-sectional bed sediment grain sizes had been applied, instead of the average grain size of bed load.

Overall, the direction of the correlation between the parameters varies between years and between cross-sections. The detected great variation in the flow characteristics within the meander bend explains why the correlation values for each mid-winter condition are so low (Table 5). Thus, the near-bed velocity and the thresholds for sediment transport conditions are highly variable throughout the meander bend. However, they are most consistent at the apex area, and there is an impact of the overall discharge on the spatial variation of the parameters.

4.2. Sediment transport capacity during varying mid-winter conditions

The shear velocities exceeded the critical shear velocities, i.e. transport stage parameter had been positive at all cross-section, at least in some measurement verticals, in 2016, 2017 and 2021 (Fig. 4, Supplementary material). The shear velocity had been greater than critical shear velocity at least in one measurement vertical each year at cs1, csA, cs2 and csB. Most often (i.e. at all or most of the measurement verticals) the threshold value had been exceeded in 2016, 2017, 2020 at cs1, and csB. Also these years, the threshold value had been exceeded at multiple measurement verticals at csA and cs2. Also in 2021, the transport stage parameter had been positive at multiple measurement verticals at cs1, csA, cs2 and csB. The shear velocity did not exceed the critical shear velocity at all in 2019 at cs3, csC or cs4. In 2018, the shear velocity did not exceed the threshold of sediment transport at any measurement vertical at csC and cs4, and in 2020 at cs3 and csC. Thus, overall, this indicates that least transport occurred at csC during different years.

Whether the applied D_{50} value had been based on the average bed load samples (Helley-Smith) or on the cross-sectional bulk bed sediment samples (Van Veen) in the calculations of years 2020 and 2021, affected the values of shear velocity and transport stage parameter (cf. Supplementary material). However, despite there were differences in the values, it only little affected whether or not the critical shear velocity threshold had been exceeded. In 2021, only in the following measurement vertical drill holes the threshold was not anymore exceeded, if the cross-sectional particle size had been applied, instead of the particle size of bed load samples (cf. Supplementary material): drill holes 7 and 12 at cs1, drill hole 10 at cs3, drill holes 2, 3 and 4 at cs4. At drill hole 13 of csA, the difference was opposite, i.e. the threshold was exceeded in 2021 when cross-sectional sediment data was applied instead of the grain size of the sampled bed load. In 2020, the critical shear velocity threshold was not exceeded anymore only at drill hole 9 of cs1 and at drill holes 12 and 16 of cs 4, when cross-sectional sediment data was applied. Note that cross-sections cs2, csB and csC had similar spatial variation of excess shear velocity over the critical shear velocity threshold in both 2020 and 2021 years independent of the applied grain size.

In addition to analysing exceeding of the critical shear velocities, the near-bed flow velocities were detected against the Hjulström (1935) diagram of critical velocities for erosion and transport. The Hjulström critical velocity for transport (0.035 m/s) was exceeded in most of the measurement locations, as the near-bed velocities were higher than that each year (Fig. 3). The velocity of 0.275 m/s, which is the critical velocity for erosion according to Hjulström (1935), would have been exceeded at least in one measurement vertical of the inlet area (i.e. cs1, csA and cs2) in each year except 2019. During mid-winter 2019, the exceeding would have occurred from those upstream cross-sections only at cs1 and cs2. However, in that year at csB as well, the critical velocity

Table 6
The Pearson correlation coefficients between different parameters at each cross-section. The depth in the calculations is the full water depth (below ice) of the measurement vertical. The values of 0.5 and higher have been bolded.

	Year	Depth vs ice thickness	Depth vs near bed velocity	Depth vs shear velocity	Depth vs transport stage parameter	Ice thickness vs near-bed velocity	Ice thickness vs shear velocity	Ice thickness vs transport stage parameter
					Average D_{50} of bedload samples used			
CS1	2016	**0.86**	**0.95**	**0.91**	**0.89**	**−0.91**	**−0.85**	**−0.79**
	2017	**−0.52**	0.05	0.10	0.16	−0.47	**−0.50**	−0.44
	2018	−0.20	0.42	0.40	0.39	−0.41	−0.45	−0.46
	2019	−0.47	**0.54**	0.49	0.47	0.00	0.04	−0.03
	2020	−0.04	**−0.63**	**−0.61**	**−0.59**	0.47	0.44	0.39
	2021	**0.82**	0.10	0.03	0.03	−0.30	−0.30	−0.26
CSA	2016	**0.66**	0.20	0.06	0.12	0.46	0.35	0.36
	2017	0.00	**−0.58**	**−0.50**	−0.32	**−0.50**	−0.49	−0.36
	2018	−0.28	−0.22	−0.28	−0.26	−0.07	−0.09	−0.18
	2019	−0.07	−0.28	−0.27	−0.15	0.41	0.45	0.53
	2020	**0.52**	−0.25	−0.29	−0.09	−0.16	−0.23	−0.04
	2021	0.43	0.37	0.27	0.30	−0.15	−0.23	−0.16
CS2	2016	−0.32	**0.89**	**0.92**	**0.94**	**−0.56**	**−0.53**	**−0.57**
	2017	**−0.80**	**0.83**	**0.69**	**0.69**	**−0.51**	−0.32	−0.31
	2018	**−0.52**	0.17	0.09	−0.03	0.06	0.11	0.32
	2019	**0.77**	0.32	0.16	0.03	0.17	0.00	−0.10
	2020	0.47	−0.43	−0.46	−0.36	**−0.59**	**−0.60**	−0.48
	2021	0.46	−0.05	−0.14	−0.18	−0.10	−0.10	−0.10
CSB	2016	−0.05	**0.80**	**0.74**	**0.64**	**−0.55**	−0.39	−0.32
	2017	**−0.82**	**0.91**	**0.62**	0.37	**−0.65**	−0.27	−0.06
	2018	**−0.87**	**0.85**	**0.84**	**0.70**	**−0.84**	**−0.83**	**−0.73**
	2019	**0.75**	**−0.53**	**−0.53**	**−0.59**	−0.25	−0.25	−0.36
	2020	**−0.95**	**0.90**	**0.86**	**0.79**	**−0.83**	**−0.77**	**−0.72**
	2021	**0.86**	0.07	−0.04	−0.01	−0.26	−0.13	−0.06
CS3	2016	−0.11	0.21	0.00	−0.16	0.15	0.07	0.01
	2017	**−0.66**	0.40	0.22	0.25	0.09	0.21	0.09
	2018	**−0.93**	0.08	0.04	0.23	0.03	0.08	−0.07
	2019	**−0.79**	0.53	0.45	0.49	**−0.85**	**−0.80**	**−0.84**
	2020	−0.47	−0.45	**−0.56**	−0.49	−0.42	−0.29	−0.33
	2021	−0.08	**0.60**	0.39	0.49	**−0.51**	−0.20	−0.19
CSC	2016	**−0.94**	0.28	0.29	0.26	−0.34	−0.34	−0.31
	2017	**0.93**	0.18	0.20	0.16	−0.07	−0.05	−0.08
	2018	−0.16	0.41	0.36	0.37	−0.28	−0.29	−0.43
	2019	**0.66**	−0.29	−0.18	−0.12	−0.07	−0.01	−0.05
	2020	−0.03	−0.31	−0.35	−0.30	0.32	0.33	0.40
	2021	0.39	**0.61**	**0.51**	0.48	**0.53**	0.45	0.46
CS4	2016	**0.54**	−0.10	−0.45	−0.46	−0.46	−0.22	−0.09
	2017	0.03	−0.06	−0.07	−0.10	−0.01	−0.04	0.01
	2018	**−0.85**	0.42	0.40	0.40	**−0.61**	**−0.62**	**−0.59**
	2019	0.24	−0.35	−0.43	−0.35	−0.42	−0.39	−0.45
	2020	**−0.60**	0.16	0.19	0.04	0.29	0.27	0.34
	2021	−0.38	−0.42	−0.48	**−0.59**	0.46	0.41	0.39
					Cross-sectional D_{50} used			
CS1	2020			**−0.62**	**−0.59**		0.44	0.39
	2021			0.04	0.03		−0.30	−0.26
CSA	2020			−0.29	−0.10		−0.23	−0.05
	2021			0.26	0.29		−0.23	−0.17
CS2	2020			−0.46	−0.36		**−0.60**	−0.48
	2021			−0.15	−0.18		−0.10	−0.10
CSB	2020			**0.86**	**0.79**		**−0.77**	**−0.72**
	2021			−0.04	−0.01		−0.13	−0.06
CS3	2020			**−0.55**	−0.48		−0.30	−0.35
	2021			0.41	**0.53**		−0.23	−0.24
CSC	2020			−0.35	−0.30		0.34	0.41
	2021			**0.50**	0.48		0.45	0.46
CS4	2020			0.19	0.04		0.27	0.34
	2021			−0.48	**−0.58**		0.41	0.40

for erosion would have been exceeded close to the inner bank side (Fig. 2). In addition to the inlet area's cross-sections, the exceeding of the critical velocity threshold for erosion would have taken place in 2020 also at csB and cs4 and in 2018 at csB. In 2016, this threshold was actually exceeded in each measurement cross-section, and in 2017, at all other cross-sections except at cs4 of the outlet area. This large amount of measurement verticals, where the exceeding of 0.275 m/s would have taken place, coincides with the years having the highest mid-winter discharges (i.e. ~1.3 m^3/s, cf. Table 1).

The bedload transport measurements with the Helley-Smith sampler

support this, as they show that during each of their measurement time (i.e. in mid-winter 2021 and 2020), the bedload was possible to measure from cs1 and cs4, and in 2021 also from cs2. Most often sampling was possible from cs1. These measurement locations coincide with the maximum velocities measured in many years (Fig. 3), i.e. the Helley-Smith measurements were done in the middle or at the left bank side at cs1 and at the outer bank at cs2 and cs4. Note that no bedload sample large enough for sieving had been collected from cs3. This coincides with the location where the flow changes from narrow csB towards the wider cross-sections of cs3–cs4 and where the near-bed velocities had been lower in mid-winter 2020 and 2021 when compared to the upstream sections. Also based on the transport stage parameter, no sediment transport would have occurred at cs3 in 2020, and only in one measurement vertical in 2021.

5. Discussion

Based on analyses done with a six-year-long flow velocity data time series (2016–2021) and two years of bedload data (2020–2021), it has been verified that despite the ice cover, there is bed sediment transport even during these harshest mid-winter conditions at this subarctic river having bed material particles of ~0.56 mm. The present study adds to the previously studied low and high open-channel flow conditions at the same study site (cf. Kasvi et al., 2013; Lotsari et al., 2020b) and gives proof that sediment transport occurs during each season. This also suggests that the ice cover should be included in future simulations in rivers having seasonal ice cover, and the sediment transport over winter should not be ignored in future change studies. Lotsari et al. (2019a) had stated—based on both simulation and measurement results gained in previous years at the same Pulmanki River study site—that the extent of the areas where critical velocities are exceeded is reduced due to ice cover when compared to open-channel situations. (Note: there were fewer measurement cross-sections in the 2013 open-channel flow period and 2014 mid-winter than in the present study.) Despite this reduction, the modelling approach of Lotsari et al. (2019a) had shown that there is sediment transport in winter conditions, similarly as in the present study done based on data from 2016 to 2021. The discharges of the Lotsari et al. (2019a) study were 0.63 m^3/s and thus close to the ones during the 'intermediate' discharge year 2019 (0.61 m^3/s) of the present study. According to Hirschfield and Sui (2011), the maximum flow velocity under ice cover depends on the roughness coefficients of the ice cover and the bed material, and the location of maximum flow velocity will be closer to the surface with the smallest resistance coefficient. Despite the ice cover being categorised as 'smooth-rough' in the Pulmanki River, the near-bed flow velocities had been enough for moving sediment particles, in particular at the inlet and apex area of the meander bend each winter.

Three different situations were possible for describing the sediment transport and near-bed velocity conditions during 2016–2021: (1) 'high' measured mid-winter discharges indicate sediment transport potential and high near-bed velocities throughout the meander bend; (2) 'low' measured mid-winter discharges indicate low near-bed velocities and sediment transport potential throughout the meander bend; (3) winters having 'intermediate' discharges indicate near-bed velocities and sediment transport potential being higher at the upstream inlet and apex sections of the meander bend, but clearly lower downstream of the apex. The near-bed velocities were the highest at the upstream inlet section of the studied symmetrical meander bend, where the measurement cross-sections were narrow and shallow, and velocities were less in the deeper and wider cross-sections of the outlet area.

The confinement of the channel by the river ice cover (i.e. bottom-fast ice) can explain the velocity variation in the case of the present study, especially during the years when the discharge had been 'intermediate'. This statement is consistent with previous studies by Kämäri et al. (2017) and Lotsari et al. (2017, 2019a) that the ice-covered high flows concentrated on narrower areas due to ice extents. They had also shown that the spatial differences in high and low flow locations increased when compared to open-channel conditions. In the present study, it was possible to show that between years, there had also been a variation in the high flow locations, especially when the mid-channel bars had affected the flow diversion around the two sides of the mid-channel bar. On the other hand, the deep and narrowest cross-section at the apex area had shown the least differences between years, and it also had in most of the mid-winters of 2016–2021 high correlation coefficient values when near-bed velocities, the ice-thickness and depth were compared to each other. The correlation between ice thickness and the near-bed velocities was negative at that location each year. Thus, the greater the velocity, the thinner the ice had been at that location. Kämäri et al. (2017) had also observed this in the same study bend but in the case of depth-averaged velocities—that is, the increase in water flow velocity decreases the ice thickness in each cross-section. Furthermore, however, the positive correlation was found between depth and near-bed velocity at the apex location during most mid-winters—except in 2019, when it was −0.53. Also, depth and ice thickness had a positive correlation in 2019 and 2021 at the meander bend apex of the Pulmanki River but a negative correlation in 2017, 2018 and 2022. Thus, the greater the depth, the greater the near-bed velocity; but most often, the ice thickness is less when greater depths occur. Wang et al. (2008) observed in their laboratory experiments that the higher the flow velocities are needed for the incipient motion of bed material, the deeper the flow depth is under ice cover. Our study indicates overall, as the depth had positive correlation with near-bed velocity and transport stage parameter in most of the analysed cross-sections and years (except at csA and cs4), that the greater the depth the greater the near-bed velocity and transport capacity are.

The largest bedload transport (Helley-Smith bedload measurements) had been measured at the upstream cross-section, which had the shallowest depths and mid-channel bars narrowing the flow area but high flow velocities. However, also the deeper cross-sections—located downstream of the apex—had bedload transport. Thus, this supports the above observations. The mechanical bedload samples should always be taken with some reservations due to the possibility of measurement errors (Helley and Smith, 1971). Also, Gaeuman and Jacobson (2006) have shown that the squared product-moment correlation coefficient (r^2) has been only 0.33 between the Helley-Smith bedload capture rate (kg/s) and the bedload velocity (m/s), thus including scatter. Ancey (2020) listed reasons why bedload transport is difficult to predict, among them being 'the mix of fast and slow processes', 'nonequilibrium and noise-driven processes', 'cascades of interacting processes', 'the varying temporal and spatial scales dependent on flow conditions', 'the heterogeneity of materials and flow conditions' and 'difficulties in obtaining reliable measurements'. In the present study, the variation in the velocities between ice-covered mid-winters of 2016–2021 underlines especially the heterogeneity of flow conditions. The near-bed velocity and the thresholds for sediment transport conditions were highly variable throughout the meander bend. However, they were most consistent at the apex area, and there was an impact of the overall discharge on the spatial variation of the parameters. Factors affecting bedload have been analysed more in open-channel conditions. As an example, a study done in an open-channel flume (Khosravi et al., 2021) found that the discharge would be the third significant factor affecting bedload transport, the most significant impact being flow velocity, followed by shear stress, discharge, bed shear velocity, bed slope, flow depth, median sediment diameter and (finally) relative roughness. Many studies have concentrated only on suspended sediment transport in ice-covered conditions (Moore et al., 2013; Weiss et al., 2015) and thus are not directly comparable to the present study.

The observed and calculated flow characteristics show that there is sediment transport potential each mid-winter at this small subarctic river flowing towards the Arctic Ocean. Based on the results, the near-bed flow velocities of up to ~0.35 m/s are expected to be able to transport the bedload in the coldest mid-winter conditions in meandering rivers having 'slightly gravelly sand' as their material sizes,

similar to the Pulmanki River. The strength of the present study is that multiple years of flow observations were possible to apply from the same cross-sectional locations and that transport occurs, especially at inlet and apex locations, despite spatial and temporal variations in ice and flow velocity conditions. Under the expected future shortening of the frozen period (Prowse et al., 2011; Turcotte et al., 2011; Lind et al., 2016), changes in bed sediment transport are also expected. Based on these mid-winter conditions, the models used for future sediment transport simulations could be validated in more detail than previously. Thus, the next step is to detect whether or not the current simulation approaches will be able to produce the observed transport conditions or if changes in the modelling approaches and fine-tuning of the equations are needed. Continuing the measurement at the Pulmanki River and different seasonally ice-covered rivers and their long-term data series would enable such better validated future analyses.

In this present study, it was only possible to analyse one meander bend, which was symmetrical in its shape and therefore represents only one type of river reach. To fully understand the sediment transport processes, the river reaches having different characteristics (e.g. varying curvature and braiding [Urroz and Ettema, 1994]) would also need to be analysed. We had not yet included the curvature in our analyses as there is ongoing research by the authors, where the flow directions (and effect of curvature on them) and also the spatial analyses are further considered in more detail. The larger the river system is, detailed consecutive measurements become more difficult, especially in ice-covered conditions. The data analysed in the present study enabled the application of simple sediment transport potential analyses. And further analyses based on the densimetric Froude number, impacts of the ice-cover roughness parameter (Namaee and Sui, 2019), or impacts of fluid viscosity (incl. water temperature) would give further insight into the flow processes in varying mid-winter sediment transport conditions.

The Pulmanki River had had smooth-rough ice cover during the analysed years when defined visually, following Demers et al. (2013), Lotsari et al. (2017) and Kämäri et al. (2017). However, more detailed roughness analyses, for example via underwater photogrammetry, would be important. Next step and undergoing work is also to analyse any possible sampling error of mechanical bed load measurements in ice-covered conditions (multiple measurements of bedload with different methods), for further developing winter time ice-covered measurements. However, this data is not yet available for this present paper. Therefore, to gain these results of roughness impact and bedload, both laboratory and field measurements are needed together to get further information on these different sediment transport conditions affecting different types of reaches. The difficulties in wintertime field measurements could also be overcome in the future when measurement techniques develop further and autonomous measurement methods (e.g. underwater remote sensing) and long-term observation stations enable analyses of spatially wider and temporally longer ice-covered flow processes.

6. Conclusions

The comparison between the mid-winter conditions in 2016–2021 showed that there is great variation in near-bed velocities between winters—but also spatially within a meander bend. However, the velocities of mid-winter conditions exceeded the requirements for particle motion each year (2016–2021) at inlet and apex area of a meander bend at the Pulmanki River, but also at the outlet area during years having discharges classified as high or intermediate. It was possible to detect three different types of situations regarding the sediment transport and near-bed velocity conditions: (1) rather similar higher flow and transport conditions throughout the meander bend during the years having the two highest overall discharges; (2) low velocities throughout the meander bend during the mid-winter having the lowest discharge. However, even during that year, the shear velocities required for sediment transport were exceeded at least in some measurement verticals of most of the cross-sections; (3) During the years of intermediate discharges, the velocities and sediment transport potential were higher at the upstream inlet and apex sections of the meander bend but clearly lower downstream of the apex.

The confinement of the channel by the river ice cover, i.e. bedfast ice, explains the velocity variation. The near-bed velocities were highest at the upstream inlet section of a symmetrical meander bend, where the measurement cross-sections were shallower. The velocities were lowest in the cross-sections located downstream of the apex, where the channel changed from relatively narrow to relatively wide. At the apex, the narrowest cross-section had the highest correlation in most of the analysed mid-winters of 2016–2021 between depth, as explanatory factor, and near-bed velocity, shear velocity and the transport stage parameter. The correlation was showing in most years (at each cross-section) negative values when near bed velocities and transport stage parameters were compared to ice-thickness. Instead, in most years positive values occurred when near bed velocities and transport stage parameter had been analysed against depth (except at csA and cs4).

The study showed that there is bedload transport despite low overall discharges during mid-winter conditions of a small (circa 20 m wide) subarctic meandering river. Based on the results, the near-bed flow velocities of up to ~0.35 m/s are expected to be able to transport bedload in the coldest mid-winter conditions in meandering rivers having 'slightly gravelly sand' as their material sizes, similar to the Pulmanki River. This should be taken into account in future analyses of the changing winter conditions on sediment transport to the Arctic Ocean, especially in the case of larger river systems having similar sand-sized river channel bed material. The gathered data and knowledge of the transportation locations, amounts and conditions enable better calibration and validation of models used for future sediment transport simulations.

CRediT authorship contribution statement

Eliisa Lotsari: Conceptualization, Data curation, Formal analysis, Funding acquisition, Investigation, Methodology, Project administration, Resources, Supervision, Validation, Visualization, Writing – original draft, Writing – review & editing. **Karoliina Lintunen:** Data curation, Formal analysis, Investigation, Methodology, Validation, Visualization, Writing – original draft, Writing – review & editing. **Elina Kasvi:** Data curation, Writing – review & editing. **Petteri Alho:** Data curation, Funding acquisition, Resources, Writing – review & editing. **Linnea Blåfield:** Data curation, Writing – review & editing.

Declaration of Competing Interest

The authors declare that they have no known competing financial interests or personal relationships that could have appeared to influence the work reported in this paper.

Data availability

The data set of this study is shared as Supplementary material (Excel file format).

Acknowledgements

We would like to thank Dr Maria Kämäri, MSc Franziska Wolff, MSc Mariana Verdonen, MSc Tiia Tarsa and MSc Marko Kärkkäinen from the University of Eastern Finland, William Speirs from the University of Queensland (Brisbane, Australia), Dr Carlos Gonzales-Inca and MSc Jouni Salmela from the University of Turku and Dr Nikita Tananaev (Melnikov Permafrost Institute [MPI] at Yakutsk, Russia) for their valuable fieldwork assistance in 2016–2021. We also thank Marko Kärkkäinen for analysing the bedload transport amounts and grain sizes and processing the orthomosaic image from the aerial photos of

February 2021. It would not have been possible to conduct the fieldwork without the drilling assistance of Ilkka Syvänperä and Esa Karpoff from the Kevo Subarctic Research Institute of University of Turku during 2016–2021. The authors have no conflicts of interest to declare.

Funding

The ice-covered flow measurements were initiated under the post-doctoral research project of Dr Lotsari, funded by the Academy of Finland (ExRIVER: grant number 267345). The work for this paper was also supported financially by four other Academy of Finland funded projects (DefrostingRivers: 338480; HYDRO-RDI-Network: 337394 and 337279; InfraRiver: 296090; Green-Digi-Basin 347701). Funding was received from the Maj and Tor Nessling Foundation (ExRIVER, grant numbers: 201300067 and 201500046; Influence of river ice and fluvial processes on river environments now and in the future, grant number: 201600042) and Strategic Research Council at the Academy of Finland (Competence-Based Growth Through Integrated Disruptive Technologies of 3D Digitalization, RobotiCS, Geospatial Information and Image Processing/Computing – Point Cloud Ecosystem, grant number: 293389). The Department of Geographical and Historical Studies, University of Eastern Finland, supported the work financially. Funding was also received from the British Society for Geomorphology (research project title 'Defrosting sedimentary systems: the impacts on the evolution and material transport of high-latitude rivers' [registered charity number: 1054260]).

Appendix A. Supplementary material

Supplementary data to this article can be found online at https://doi.org/10.1016/j.jhydrol.2022.128610.

References

Ancey, C., 2020. Bedload transport: a walk between randomness and determinism. Part 1. The state of the art. J. Hydraul. Res. 58, 1–17. https://doi.org/10.1080/00221686.2019.1702594.

Autio, J., Heikkinen, O., 2002. The Climate of Northern Finland. Fennia 180, 61–66.

Beltaos, S., Burrell, B.C., 2016. Transport of suspended sediment during the breakup of the ice cover, Saint John River, Canada. Cold Reg. Sci. Technol. 129, 1–13. https://doi.org/10.1016/j.coldregions.2016.05.006.

Biron, P.M., Buffin-Belanger, T., Martel, N., 2019. Three-dimensional turbulent structures at a medium-sized confluence with and without an ice cover. Earth Surf. Proc. Land. 44 (15), 3042–3056. https://doi.org/10.1002/esp.4718.

Demers, S., Buffin-Bélanger, T., Roy, A.G., 2011. Helical cell motions in a small ice-covered meander river reach. River Res. Appl. 27, 1118–1125. https://doi.org/10.1002/rra.1451.

Demers, S., Buffin-Bélanger, T., Roy, A.G., 2013. Macroturbulent coherent structures in an ice-covered river flow using a pulse-coherent acoustic Doppler profiler. Earth Surf. Proc. Land. 38, 937–946. https://doi.org/10.1002/esp.3334.

Ettema, R., Daly, S.F., 2004. Sediment Transport Under Ice. ERDC/CRREL TR-04-20. US Army Corps of Engineers, Cold Regions Research and Engineering Laboratory, New Hampshire, USA, pp. 1–54.

Gaeuman, D., Jacobson, R.B., 2006. Acoustic bed velocity and bed load dynamics in a large sand bed river. J. Geophys. Res. 111, F02005. https://doi.org/10.1029/2005JF000411.

Helley, E.J., Smith, W., 1971. Development and calibration of a pressure-difference bedload sampler. U.S. Geological Survey Open-File Report. U.S. Dept. of the Interior, Geological Survey, Water Resources Division: Menlo Park, California, USA. 18 p.

Hirschfield, F., Sui, J., 2011. Sediment Transport under Ice Conditions. In: Ginsberg, S.S. (Ed.), Sediment transport. IntechOpen, London, UK, pp. 261–274.

Hirshfield, F., Sui, J., 2011. Sediment Transport under Ice Conditions. In: Ginsberg, S.S. (Ed.), Sediment Transport. InTech. https://doi.org/10.5772/16114.

Hirvas, H., Lagerback, R., Mäkinen, K., Nenonen, K., Olsen, L., Rodhe, L., Thoresen, M., 1988. The Nordkalott Project: studies of Quaternary ge-ology in northern Fennoscandia. Boreas 17, 431–437. https://doi.org/10.1111/j.1502-3885.1988.tb00560.x.

Hjulström, F., 1935. Studies of morphological activity of rivers as illustrated by the River Fyris. Bull. Geol. Inst. Univ. Uppsala 25, 221–527.

IPCC, 2021. Summary for Policymakers. In: Masson-Delmotte, V.P., et al. (Eds.), Climate Change 2021: The Physical Science Basis. Contribution of Working Group I to the Sixth Assessment Report of the Intergovernmental Panel on Climate Change. Cambridge University Press. In Press.

Johansson, P., 1995. The deglaciation in the eastern part of the Weichsalian ice divide in Finnish Lapland. Geol. Surv. Finland, Bull. 383, 1–72.

Johansson, P., 2007. Late Weichselian deglaciation in Finnish Lapland. Applied Quaternary research in the central part of glaciated terrain. Geol. Surv. Finland Spec. Pap. 46, 47–54.

Kämäri, M., Alho, P., Veijalainen, N., Aaltonen, J., Huokuna, M., Lotsari, E., 2015. River ice cover influence on sediment transportation at present and under projected hydro-climatic conditions. Hydr. Process. 29, 4738–4755. https://doi.org/10.1002/hyp.10522.

Kämäri, M., Alho, P., Colpaert, A., Lotsari, E., 2017. Spatial variation of river-ice thickness in a meandering river. Cold Reg. Sci. Technol. 137, 17–29. https://doi.org/10.1016/j.coldregions.2017.01.009.

Kämäri, M., Tattari, S., Lotsari, E., Koskiaho, J., Lloyd, C.E.M., 2018. High-frequency monitoring reveals seasonal and event-scale water quality variation in a temporally frozen river. J. Hydrol. 564, 619–639. https://doi.org/10.1016/j.jhydrol.2018.07.037.

Kasvi, E., Vaaja, M., Alho, P., Hyyppä, H., Hyyppä, J., Kaartinen, H., Kukko, A., 2013. Morphological changes on meander point bars associated with flow structure at different discharges. Earth Surf. Process. Landf. 38, 577–590. https://doi.org/10.1002/esp.3303.

Kestin, J., Sokolov, M., Wakeham, W.A., 1978. Viscosity of liquid water in the range −8 °C to 150 °C. J. Phys. Chem. Ref. Data 7, 941–948. https://doi.org/10.1063/1.555581.

Khosravi, K., Cooper, J.R., Daggupati, P., Pham, B.T., Bui, D.T., 2021. Bedload transport rate prediction: Application of novel hybrid data mining techniques. J. Hydrol. 585, 124774 https://doi.org/10.1016/j.jhydrol.2020.124774.

Ladegaard-Pedersen, P., Sigsgaard, C., Kroon, A., Abermann, J., Skov, K., Elberling, B., 2017. Suspended sediment in a high-Arctic river: An appraisal of flux estimation methods. Sci. Total Environ. 580, 582–592. https://doi.org/10.1016/j.scitotenv.2016.12.006.

Lewis, T., Lamoureux, S., 2010. Twenty-first century discharge and sediment yield predictions in a small high Arctic watershed. Global Planet. Change 71, 27–41. https://doi.org/10.1016/j.gloplacha.2009.12.006.

Lind, L., Alfredsen, K., Kuglerová, L., Nilsson, C., 2016. Hydrological and thermal controls of ice formation in 25 boreal stream reaches. J. Hydrol. 540, 797–811. https://doi.org/10.1016/j.jhydrol.2016.06.053.

Lotsari, E., Vaaja, M., Flener, C., Kaartinen, H., Kukko, A., Kasvi, E., Hyyppä, H., Hyyppä, J., Alho, P., 2014. Annual bank and point bar morphodynamics of a meandering river determined by high-accuracy multitemporal laser scanning and flow data. Water Resour. Res. 50, 5532–5559. https://doi.org/10.1002/2013WR014106.

Lotsari, E., Thorndycraft, V., Alho, P., 2015a. Prospects and challenges of simulating river channel response to future climate change. Prog. Phys. Geogr. 39, 483–513. https://doi.org/10.1177/0309133315578944.

Lotsari, E., Wang, Y., Kaartinen, H., Jaakkola, A., Kukko, A., Vaaja, M., Hyyppä, H., Hyyppä, J., Alho, P., 2015b. Gravel transport by ice in a subarctic river from accurate laser scanning. Geomorphology 246, 113–122. https://doi.org/10.1016/j.geomorph.2015.06.009.

Lotsari, E., Kasvi, E., Kämäri, M., Alho, P., 2017. The effects of ice-cover on flow characteristics in a subarctic meandering river. Earth Surf. Process. Landf. 42, 1195–1212. https://doi.org/10.1002/esp.4089.

Lotsari, E., Tarsa, T., Kämäri, M., Alho, P., Kasvi, E., 2019a. Spatial variation of flow characteristics in a subarctic meandering river in ice-covered and open-channel conditions: 2D hydrodynamic modelling approach. Earth Surf. Process. Landf. 44, 1509–1529. https://doi.org/10.1002/esp.4589.

Lotsari, E., Hackney, C., Salmela, J., Kasvi, E., Kemp, J., Alho, P., Darby, S., 2020a. Subarctic river bank dynamics and driving processes during the open-channel flow period. Earth Surf. Process. Landf. 45, 1198–1216. https://doi.org/10.1002/esp.4796.

Lotsari, E., Dietze, M., Kämäri, M., Alho, P., Kasvi, E., 2020b. Macro-Turbulent Flow and Its Impacts on Sediment Transport Potential of a Subarctic River during Ice-Covered and Open-Channel Conditions. Water 12, 1874. https://doi.org/10.3390/w12071874.

Lotsari, E., Lind, L., Kämäri, M., 2019b. Impacts of Hydro-Climatically Varying Years on Ice Growth and Decay in a Subarctic River. Water 11, 2058. https://doi.org/10.3390/w11102058.

Moore, S.A., Ghareh Aghaji Zare, S., Rennie, C.D., Seidou, O., Ahmari, H., 2013. Monitoring suspended sediment under ice using acoustic instruments: Presentation of measurements made under break-up, Committee on River Processes and the Environment, proceedings of 17th Workshop on river ice, Canadian Geophysical Union, Edmonton, Alberta, Canada.

Morales, J.A., Lozano, C., Sedrati, M., 2019. Calculated Potential Bedload Versus Real Transported Sands along the Guadiana River Estuary (Spain–Portugal). J. Marine Sci. Eng. 7, 393, 21 pp. https://doi.org/10.3390/jmse7110393.

Namaee, M.R., Sui, J., 2019. Effects of ice cover on the incipient motion of bed material and shear stress around side-by-side bridge piers. Cold Regions Sci. Technol. 165 (102811), 1–14. https://doi.org/10.1016/j.coldregions.2019.102811.

Peel, M.C., Finlayson, B.L., McMahon, T.A., 2007. Updated world map of the Köppen-Geiger climate classification. Hydrol. Earth Syst. Sci. 11, 1633–1644. https://doi.org/10.5194/hess-11-1633-2007.

Polvi, L.E., Dietze, M., Lotsari, E., Turowski, J.M., Lind, L., 2020. Seismic Monitoring of a Subarctic River: Seasonal Variations in Hydraulics, Sediment Transport, and Ice Dynamics. e2019JF005333 J. Geophys. Res.: Earth Surf. 125. https://doi.org/10.1029/2019JF005333.

Poutanen, M., Bilker-Koivula, M., Ruotsalainen, H. 2017. Acceleration of free fall. NLS (National Land Survey of Finland) Finnish Geospatial Research Institute FGI. VTT MIKES METROLOGY Calibration services 2016. 16–17 pp. https://www.maanmitta

uslaitos.fi/sites/maanmittauslaitos.fi/files/attachments/2017/05/calibration_acceleration_of_free_fall.pdf.
Prowse, T.D., 1993. Suspended sediment concentration during river ice breakup. Can. J. Civ. Eng. 20, 872–875. https://doi.org/10.1139/l93-113.
Prowse, T.D., Alfredsen, K., Beltaos, S., Bonsal, B.R., Bowden, W.B., Duguay, C.R., Korhola, A., McNamara, J., Vincent, W.F., Vuglinsky, V., Anthony, K.M.W., Weyhenmeyer, G.A., 2011. Effects of Changes in Arctic Lake and River Ice. Ambio 40, 63–74. https://doi.org/10.1007/s13280-011-0217-6.
Prowse, T.D., 1996. Significance of River Ice to Environmental Processes and Aquatic Ecosystems. In: Proceedings of the 13th International Symposium on Ice, IAHR, Beijing, China. August 27–31, 1996 3, pp. 865–872.
Rennie, C.D., Millar, R.G., Church, M.A., 2002. Measurement of bedload velocity using an acoustic Doppler current profiler. J. Hydraulic Eng. 128, 473–483. https://doi.org/10.1061/(ASCE)0733-9429(2002)128:5(473).
Rennie, C.D., Vericat, D., Williams, R.D., Brasington, J., Hicks, M., 2017. Calibration of aDcp apparent bedload velocity to bedload transport rate. In: Tsutsumi, D., Laronne, J. (Eds.), Gravel-Bed Rivers: Processes and Disasters. Wiley.
Rhoads, B.L. 2020. River dynamics. Geomorphology to support management. Cambridge University Press, United Kingdom. 515 p. https://doi.org/10.1017/9781108164108.
Shields, A., 1936. Application of similarity principles and turbulence research to bed-load movement. Mitteilunger der Preussischen Versuchsanstalt fuer Wasserbau und Schiffbau 26, 5–24.
Sime, L.C., Ferguson, R.I., Church, M., 2007. Estimating shear stress from moving boat acoustic Doppler velocity measurements in a large gravel bed river. Water Resour. Res. 43, W03418. https://doi.org/10.1029/2006WR005069.
Song, C., Wang, G., Mao, T., Dai, J., Yang, D., 2019. Linkage between permafrost distribution and river runoff changes across the Arctic and the Tibetan Plateau. Sci. China Earth Sci. 1–11 https://doi.org/10.1007/s11430-018-9383-6.
Sontek, 2015. RiverSurveyour – Discharge, bathymetry and current profiling. Brochure. Sontek, San Diego, California, USA, 4 p.
Syvitski, J., 2002. Sediment discharge variability in Arctic rivers: implications for a warmer future. Polar Res. 21, 323–330. https://doi.org/10.1111/j.1751-8369.2002.tb00087.x.
Tremblay, P., Leconte, R., Lacey, R.W.J., Bergeron, N., 2014. Multi-day anchor ice cycles and bedload transport in a gravel-bed stream. J. Hydrol. 519, 364–375. https://doi.org/10.1016/j.jhydrol.2014.06.036.
Turcotte, B., Morse, B., Bergeron, N.E., Roy, A.G., 2011. Sediment transport in ice-affected rivers. J. Hydrol. 409, 561–577. https://doi.org/10.1016/j.jhydrol.2011.08.009.
Van Rijn, L., 1984. Sediment transport, part I: Bed load transport. J. Hydraul. Eng. 110, 1431–1456. https://doi.org/10.1061/(ASCE)0733-9429(1984)110:10(1431).
Veijalainen, N., Lotsari, E., Alho, P., Vehviläinen, B., Käyhkö, J., 2010. National scale assessment of climate change impacts on flooding in Finland. J. Hydrol. 391, 333–350. https://doi.org/10.1016/j.jhydrol.2010.07.035.
Wang, J., Sui, J., Karney, B., 2008. Incipient motion of non-cohesive sediment under ice cover - an experimental study. J. Hydrodyn. 20, 117–124. https://doi.org/10.1016/S1001-6058(08)60036-0.
Weiss, A., Clark, S.P., Rennie, C.D., Moore, S.A., Ahmari, H., 2015. Estimation of total suspended solids concentration from aDcp backscatter and hydraulic measurements. J. Hydraul. Res. 53, 670–677. https://doi.org/10.1080/00221686.2015.1076531.
Wilcock, P.R., 1996. Estimating local bed shear stress from velocity observation. Water Resour. Res. 32, 3361–3366. https://doi.org/10.1029/96WR02277.
Zare, S.G.A., Moore, S.A., Rennie, C.D., Seidou, O., Ahmari, H., Malenchak, J., 2016a. Estimation of composite hydraulic resistance in ice covered alluvial streams. Water Resour. Res. 52, 1306–1327. https://doi.org/10.1002/2015WR018096.
Zare, S.G.A., Moore, S.A., Rennie, C.D., Seidou, O., Ahmari, H., Malenchak, J., 2016b. Boundary shear stress in an ice covered river during break-up. J. Hydraulic Eng. 142, 04015065. https://doi.org/10.1061/(ASCE)HY.1943-7900.0001081.